



## City Research Online

### City, University of London Institutional Repository

---

**Citation:** Soltani, M. R., Masdari, M. & Damghani, H. (2013). Experimental investigation of leading-edge roughness effects on stationary crossflow instability of a swept wing. *Scientia Iranica*, 20(3), pp. 524-534. doi: 10.1016/j.scient.2013.01.006

This is the published version of the paper.

This version of the publication may differ from the final published version.

---

**Permanent repository link:** <https://openaccess.city.ac.uk/id/eprint/32945/>

**Link to published version:** <https://doi.org/10.1016/j.scient.2013.01.006>

**Copyright:** City Research Online aims to make research outputs of City, University of London available to a wider audience. Copyright and Moral Rights remain with the author(s) and/or copyright holders. URLs from City Research Online may be freely distributed and linked to.

**Reuse:** Copies of full items can be used for personal research or study, educational, or not-for-profit purposes without prior permission or charge. Provided that the authors, title and full bibliographic details are credited, a hyperlink and/or URL is given for the original metadata page and the content is not changed in any way.

---

---

---

City Research Online:

<http://openaccess.city.ac.uk/>

[publications@city.ac.uk](mailto:publications@city.ac.uk)

---



Sharif University of Technology

Scientia Iranica

Transactions B: Mechanical Engineering

www.sciencedirect.com



Research note

# Experimental investigation of leading-edge roughness effects on stationary crossflow instability of a swept wing

M.R. Soltani, M. Masdari\*, H. Damghani

Department of Aerospace Engineering, Sharif University of Technology, Tehran, P.O. Box number: 1458889694, Iran

Received 14 March 2012; revised 9 November 2012; accepted 7 January 2013

## KEYWORDS

Swept wing;  
Pressure distribution;  
Roughness effects;  
Spectral analysis;  
Zero frequency instability.

**Abstract** Wind tunnel experiments were conducted to evaluate surface pressure distribution over a semi span swept wing with a sweep angle of  $33^\circ$ . The wing section has a laminar flow airfoil similar to that of the NACA 6-series. The tests were conducted at speeds ranging from 50 to 70 m/s with and without surface roughness. Surface static pressure was measured on the wing upper surface at three different chordwise rows located at the inboard, middle, and outboard stations. The differences between pressure distributions on the three sections of the wing were studied and the experimental results showed that roughness elements do not influence the pressure distribution significantly, except at the inboard station. On the other hand, spectral analysis of the pressure–time signals acquired from the pressure orifices over the wing upper surface showed that roughness had significantly affected the zero frequency amplitude. In this study, the zero frequency amplitude and its variations with roughness elements was investigated at three different chordwise positions; inboard, middle, and outboard stations. Results showed that the 3-D roughness elements amplified zero frequency amplitude over the wing surface. Zero frequency distribution at the inboard station, closer to the wing root, in comparison with the middle station, was reduced after an initial amplification along the chord. Moreover, the effect of roughness on the zero frequency instability at the first section was negligible due to the narrow instability amplification region. On the other hand, at the outboard station, closer to the wing tip, the instabilities were amplified over a larger region, with respect to the middle station.

© 2013 Sharif University of Technology. Production and hosting by Elsevier B.V.

Open access under CC BY-NC-ND license.

## 1. Introduction

The idea of using swept wing was first developed in Germany in the 1930s. They noticed that the critical Mach number over the wing was dominated by the normal component of the airflow, not the free stream velocity. Thus, by setting the wing at an angle, the critical Mach number could be increased, a phenomenon that leads to drag reduction. However, the drawback of this advantage was found to be related to a complicated boundary layer problem becoming three dimensional due to the wing sweep angle. To understand the effects, a considerable

amount of research, mainly experimental, were devoted to the three-dimensional swept wing boundary layer.

One of the first experiments on the three-dimensional boundary layer over a swept wing was initiated by Gray [1] at the British Royal Aircraft Academy around 1970. In his flight tests, he perceived that the boundary layer of a swept wing became turbulent much closer to the leading edge than on the corresponding unswept wing. These observations gave rise to the classical basic research work conducted by Gregory et al. [2] on a rotating disk. They identified the underlying instability mechanism as inflectional instability caused by the three-dimensional flow.

In fact, a combination of the sweep angle and pressure gradient produces curved streamlines at the boundary layer edge (Figure 1). The curved streamlines create a secondary flow that is perpendicular to the oncoming streamline and is called crossflow. The crossflow velocity profile has an inflection point that contributes to the crossflow instabilities. Crossflow instabilities are one of the principal characteristics of three-dimensional boundary layer flows. However, in swept wing

\* Corresponding author.

E-mail addresses: msoltani@sharif.edu (M.R. Soltani), mmasdari@yahoo.com (M. Masdari), hdamghani1@yahoo.com (H. Damghani).  
Peer review under responsibility of Sharif University of Technology.



Production and hosting by Elsevier

### Nomenclature

$V_\infty$	Freestream velocity ( $\frac{m}{s}$ )
$c$	Airfoil chord
$x$	Distance from the leading edge of the airfoil
$\alpha$	Angle of attack ( $^\circ$ )
$\delta$	Boundary layer thickness
$k$	Roughness height
$A$	Zero frequency amplitude at the desired point
$A_0$	Zero frequency amplitude at the reference point ( $x/c \approx 0.1$ )
$b$	Half wing span (mm)

flows, three other instabilities may exist, namely; attachment line, streamwise, and centrifugal [3]. The attachment-line problems usually develop on the swept wings that have a large leading-edge radius. The streamwise instability is similar to the Tollmien–Schlichting waves in 2-D flows, and, finally, the centrifugal instabilities depend on the concave regions over the surface. All these instabilities may exist independently or in combinations over a swept wing boundary layer.

Crossflow instabilities due to the secondary flow velocity profile are divided into stationary and travelling waves. Whether the stationary or travelling waves dominate is an important question. For this purpose, Bippes and Deyhle [4] measured and studied amplification of disturbances in the unstable three-dimensional boundary-layer flow over a swept-back flat plate. Their observations showed that with decreasing free-stream turbulence, stationary crossflow waves dominated. However, according to linear theory, the traveling mode is the most amplified one. In fact, in a high turbulence wind tunnel, the amplification rate of the zero Hz mode is very small [4,5]. Therefore, one expects low turbulence results to be more important, because the flight environment is in a very low turbulent region; even lower than the so-called laminar flow wind tunnel. In addition, they found that travelling waves are amplified by increasing the free stream turbulence for a constant surface roughness, which leads to domination of the travelling waves almost beyond  $Tu = 0.0015$ . The importance of traveling crossflow instability and its dependence on freestream conditions was further investigated by Bippes [6]. Later, White and Saric [7] investigated crossflow instabilities on an infinite swept wing. They concluded that the existence of traveling or stationary crossflow instability depends on the interaction of the freestream turbulence and surface roughness. Additionally, selection of travelling or stationary waves clearly influences the prospect for the transition prediction of the three dimensional boundary layers.

However, in many experiments, practically, the stationary mode is first observed, and, thus, more investigations have been carried out on this mode; stationary crossflow instability. Actually, at the limit of zero frequency, crossflow instabilities are stationary with respect to the surface and are called stationary crossflow instabilities. In addition, for a swept wing, these waves are nearly aligned with the inviscid streamlines. Consequently, even though amplitude of the wave is weak, it produces an integrated effect that causes a strong distortion in the mean flow velocity profile. Thus, swept wing transition prediction is not possible without studying mean flow distortion, due to the zero frequency instability, and other parameters such as 3-D surface roughness. Note that 3-D surface roughness strongly influences zero frequency

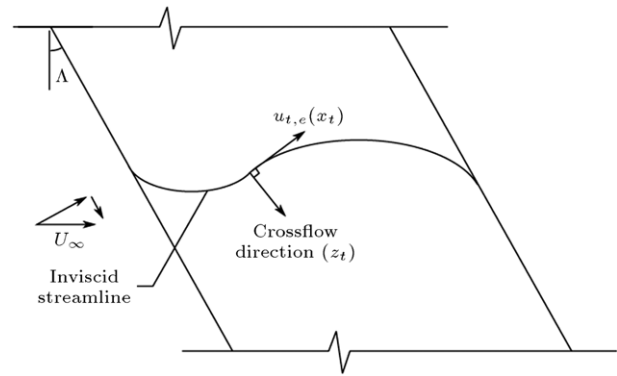


Figure 1: Schematic of an inviscid streamline over swept wing [3].

instability amplitude. Radeztsky et al. [8] investigated the effect of roughness elements on stationary crossflow instability over an infinite swept wing. They presented the effects of both roughness size and location on the transition point over a swept wing dominated by the cross flow instability. Their results showed that roughness effects seem to be confined to a small region near the attachment line, where crossflow disturbances first begin to be amplified. In addition, crossflow instability is relatively insensitive to both sound and 2-D surface roughness. In 1994, Radeztsky [9] carried out another experimental investigation on low-amplitude crossflow instability in order to compare experimental results with linear theory predictions. The crossflow vortices were amplified by applying roughness elements near the leading edge. The growth and development of the disturbances over an infinite swept wing were then documented. Their results showed that linear stability was not able to predict the growth rates of the crossflow instability accurately [9]. Riebert et al. [10] experimentally studied the effect of roughness elements on stationary crossflow instability, based on Radeztsky's work, and compared their results with both linear and NPSE theory. Their data confirmed the extreme sensitivity of the boundary layer to the leading-edge roughness. Moreover, their results showed that linear theory was not able to capture details of the disturbance growth. However, NPSE calculations agreed remarkably well with experimental data.

Carrillo [11] carried out a set of experiments, where stationary crossflow disturbance was amplified by applying subcritical roughness elements near the leading edge i.e., spacing between the roughness elements was less than the wave length of the instability over the clean surface. He reported that the transition location of the rough surface was delayed surprisingly beyond the location where it occurred in the absence of the 3-D roughness. This is because the most unstable mode was suppressed over a swept wing under these conditions. These observations encouraged researchers to study transition control by means of artificial roughness over crossflow dominated swept wings. White and Saric [12] designed a quite primitive control system by using this concept. Their system controlled transition location over swept wings by adding an array of micron-sized roughness elements near the wing leading edge.

The issue of boundary layer instabilities over a finite swept wing is still in its primitive stage and many aspects of it are yet unclear. Current experimental work is designed to broaden our knowledge of stationary crossflow instability characteristics over swept wings. In the present work, a wing with sweep angle of  $33^\circ$  was tested in a wind tunnel. Since the wing has a small leading-edge radius and there is no concave regions on the wing upper surface, attachment-line and centrifugal instability are



Figure 2: The model in the test section.

not expected. On the other hand, streamwise instability could be ignored for small angles of attack [3]. Therefore, based on these facts, crossflow instability was studied separately from other three instability modes. For these tests, surface pressure signals over the upper surface of the swept wing were measured at three different spanwise locations. The tests were conducted at three different Reynolds numbers of  $0.8 \times 10^6$ ,  $1.13 \times 10^6$  and  $1.28 \times 10^6$  and at angles of attack ranging from  $\alpha = -2^\circ$  to  $1^\circ$ . The highly polished wing surface provided a clean baseline condition and the stationary crossflow instability was amplified by gluing distributed roughness elements near the leading edge at  $x/c = 0.05$ . Roughness elements were of circular shape with an average diameter of  $200 \mu\text{m}$ , which are easy to apply and can be easily removed. The surface of elements is uneven, with variations of approximately 20%. Micron-sized roughness elements were well above the background roughness level because of the highly polished surface. Thus, roughness height was large enough to produce significant stationary crossflow amplitudes.

## 2. Experimental apparatus

All experiments were conducted in a subsonic wind tunnel of a closed return type, with a test section of  $80 \text{ cm} \times 80 \text{ cm} \times 200 \text{ cm}$ , operating at speeds from 10 to 100 m/s. The inlet of the tunnel has a 7:1 contraction ratio with four large, anti-turbulence screens and a honeycomb in its settling chamber to reduce the tunnel turbulence to less than 0.001 in the test section at a Reynolds number of  $0.8 \times 10^6$ . Furthermore, the turbulence intensity of the test section varies between 0.0009 and 0.0013 as the Reynolds number is increased from  $0.8 \times 10^6$  to  $1.28 \times 10^6$ . The model used in this experiment is a scaled model of a tapered wing whose section is similar to that of NACA6-series airfoils. Semi-span wings were designed and fabricated to achieve higher Re number during the tests. A flat plate is used at the end of the model to reduce the boundary layer effect of the test section on the model. The general arrangement of the model used for this investigation, when installed in the wind tunnel, is shown in Figure 2. The baseline configuration is a semi-span, 1/2.5 scale model of an actual wing. The model has a leading edge sweep of  $33^\circ$  and a span of 516 mm.

Hot wire anemometry is an expensive and accurate measurement method, but this measuring method is also destructive. Thus, unlike the applied method, the flow field is affected by the traverse system and thermal gradient. In addition, hot

wire is more sensitive to electronic noise and needs more data processing. On the other hand, pressure transducers, which are used in these tests, provide a cheaper and simpler method, which is also reliable for low frequency structures. Pressure signals were acquired over the wing upper surface, with a total of 61 pressure orifices of 0.4 mm diameter, arranged in three stream wise rows, Sections 1 through 3 (Figure 3(a) and (b)). Surface pressure is sensed through HCX series transducers, fully signal conditioned pressure transducers, from SENSORTCH-NICS, with an accuracy of  $\pm 0.1\%$  full scale output and 1 kHz sample rate frequency. Each transducer data is collected via a terminal board and transformed to the computer through a 64 channel, 12-bit Analog-to-Digital (A/D) board, capable of an acquisition rate of up to 500 kHz.

Raw data are then digitally filtered using a low-pass filtering routine. During the filtering process, the cut off frequency is calculated either from the Power Spectrum Density (PSD) estimation or from the frequency domain analysis. The advantage of this method is that the noise which may dominate the signal in the time domain appears only as a single peak or spike in the frequency domain [13]. Once the frequency of the noise is determined, it is easily filtered out and a clean signal is obtained for the analysis. For this purpose, a computer program was architected and built to filter the data acquired from each sensor.

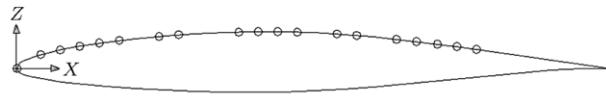
## 3. Results and discussion

Surface static pressure was measured on the wing upper surface at three different chordwise rows located at the inboard station, (Section 1,  $y/b = 0.2$ ), middle station, (Section 2,  $y/b = 0.43$ ), and outboard station, (Section 3,  $y/b = 0.78$ ), (Figure 3). The tests were conducted at tunnel speeds of  $V_\infty = 50 - 70 \text{ m/s}$  and at angles of attack ranging from  $-2^\circ$  to  $1^\circ$  for both clean and rough surfaces. The results of the pressure distribution are discussed first, followed by the results of the spectral analysis of the pressure–time signals acquired from the pressure orifices over the wing upper surface.

### 3.1. Pressure distribution

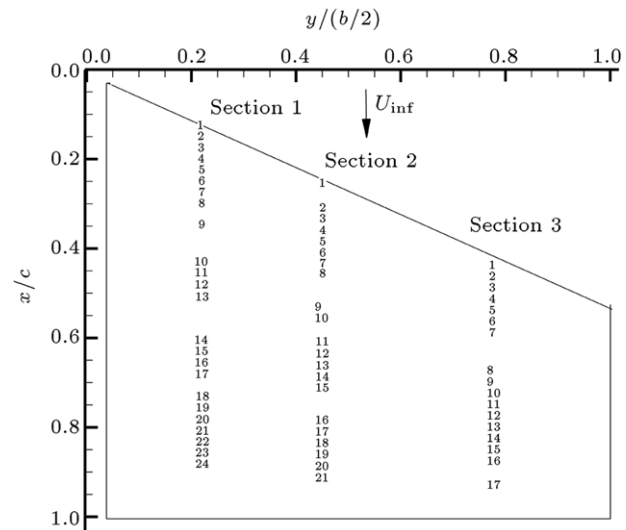
Figure 4 illustrates the effect of roughness elements on wing surface pressure distribution at three sections for angles of attack of zero degrees and for  $V_\infty = 50 \text{ m/s}$ . It is clearly seen that the roughness elements have little influence on the wing surface  $C_p$  distribution, at least for this roughness size. In addition, the most influence was observed to occur at the inboard station, Section 1.

The pressure distribution over the swept wing is more influenced by the crossflow, and for the inboard station of the present wing, the crossflow is weaker than the corresponding ones of the other two stations. Therefore, surface roughness should be more effective at this station (inboard station). Figure 5 illustrates the pressure distribution at Section 1 for different angles of attack. From this figure, it is seen that the minimum value of  $C_p$  for the rough surface at the inboard station is closer to the edge of the wing in comparison with the clean one. In other words, by studying the ratio of roughness height to boundary layer thickness (denoted by  $k/\delta$ ), at the inboard station,  $k/\delta$  has its maximum value, which results in higher blockage when the roughness is applied. Therefore, based on this analysis, in Section 1, roughness should have significant effects on the  $C_p$  distribution, whereas, at middle and outboard stations, the ratio of  $k/\delta$  became smaller



Airfoil geometry		
$x/c$	$Z_{upper}/c$	$Z_{lower}/c$
0.00	0	0
0.02	0.017	-0.013
0.05	0.026	-0.018
0.07	0.030	-0.021
0.09	0.035	-0.024
0.12	0.038	-0.027
0.14	0.042	-0.029
0.16	0.045	-0.031
0.19	0.048	-0.033
0.21	0.051	-0.034
0.23	0.053	-0.035
0.26	0.055	-0.037
0.28	0.056	-0.037
0.31	0.058	-0.038
0.35	0.060	-0.039
0.40	0.061	-0.039
0.45	0.061	-0.039
0.49	0.059	-0.037
0.54	0.056	-0.035
0.59	0.053	-0.032
0.65	0.047	-0.026
0.72	0.039	-0.020
0.79	0.029	-0.013
0.86	0.020	-0.007
0.92	0.010	-0.001
1.00	0.000	0.000

Pressure tabs		
Tab no.	$x/c$	$Z_{upper}/c$
1	0.000	0.000
2	0.074	0.031
3	0.107	0.036
4	0.140	0.042
5	0.174	0.046
6	0.207	0.050
7	0.234	0.053
8	0.261	0.055
9	0.376	0.060
10	0.409	0.061
11	0.477	0.059
12	0.510	0.057
13	0.545	0.055
14	0.578	0.053
15	0.612	0.050
16	0.713	0.038
17	0.746	0.035
18	0.780	0.030
19	0.813	0.026
20	0.847	0.022
21	0.880	0.016



(a) Positions of the surface pressure tabs at the midchord and the airfoil geometry.

(b) Chordwise rows of pressure orifices.

Figure 3: Schematic of the pressure orifices on the wing surface.

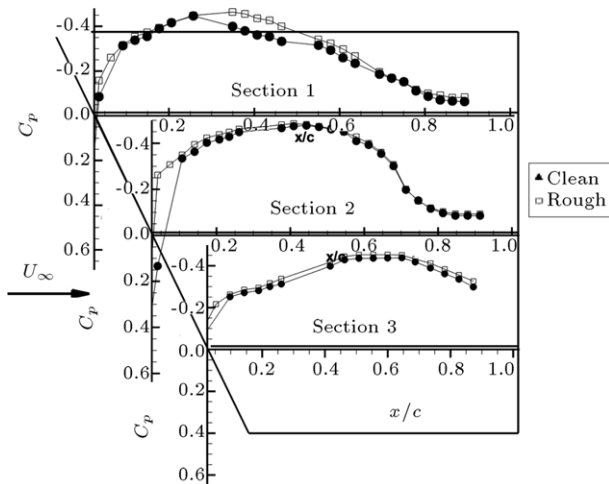


Figure 4:  $C_p$  distribution at three chordwise sections,  $\alpha = 0^\circ$ ,  $v_\infty = 50$  m/s.

and, therefore, pressure profile variations in the presence of roughness at different angles of attack are negligible, which is clearly seen by examining the pressure data shown in Figures 6 and 7. In fact, swept-wing boundary layer flow consists of a streamwise direction along the local chord, and a velocity component perpendicular to the streamwise direction along the wing span [3, 14]. Therefore, boundary layer thickness grows in two directions; along the local chord, from the leading edge to the trailing edge, and along the wing span, from the root to the tip of the wing. Moreover, boundary layer thickness was the only variable in this ratio (roughness size was identical at all sections). Hence,  $k/\delta$  decreases by moving away from the inboard to the outboard station.

### 3.2. Zero frequency instability

Zero frequency amplitude represents stationary crossflow instability over the swept wing [3]. To obtain stationary waves from the pressure signals, a power spectrum function was used. A power spectrum is useful for measuring the frequency content of the stationary or transient signals. By transforming a time-dependent pressure into the Fourier domain, one can observe active frequencies within the flow field. In addition, the evolution of the energy in the measured pressure can be obtained by observing the auto-spectra, power spectrum density, for pressure signals. These spectra were computed using the Fast Fourier Transform (FFT) function of the LABVIEW program. The windowing of the pressure signal was done by the Hanning method to decrease the amount of leakage.

Figure 8(a) illustrates the zero frequency amplitude distribution at the inboard station, section no. 1, for different angles of attack and for a freestream velocity of  $V_\infty = 50$  m/s. According to this figure, the amplitude of the zero frequency is increased by moving away from the leading edge, increasing  $x/c$ , and its maximum occurs at about  $x/c \approx 0.35$  for all angles of attack. Then, as  $x/c$  increases,  $x/c > 0.35$ , the amplitude of zero frequency decreases, followed by a sharp drop around  $x/c \approx 0.45$  and beyond. Note that for  $x/c > 0.6$ , the amplitude of the disturbance is the same for all angles of attack (Figure 8(a)). This is because the most effective parameter on the perturbation is the minimum  $C_p$  position, which occurs far from the trailing edge. Figure 8(b) and (c) illustrate the zero frequency amplitude distribution at the middle and outboard stations, Sections 2 and 3, respectively, for different angles of attack and for a freestream velocity of  $V_\infty = 50$  m/s. The variations for the middle station (Figure 8(b)), is similar to that of the inboard one shown in Figure 8(a). However, the amplitude distribution for this section is very smooth, as seen from this figure. In addition, the point of maximum amplitude is displaced and occurs at  $x/c \approx 0.4$ .

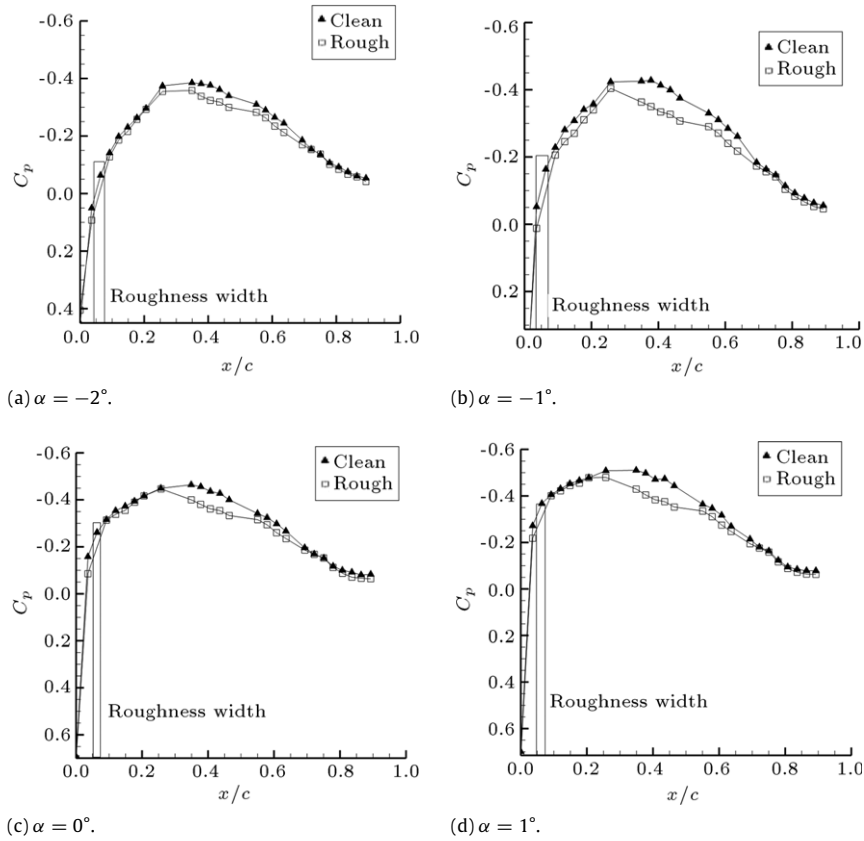


Figure 5: Effect of angle of attack on the inboard section pressure distribution,  $v_\infty = 50$  m/s.

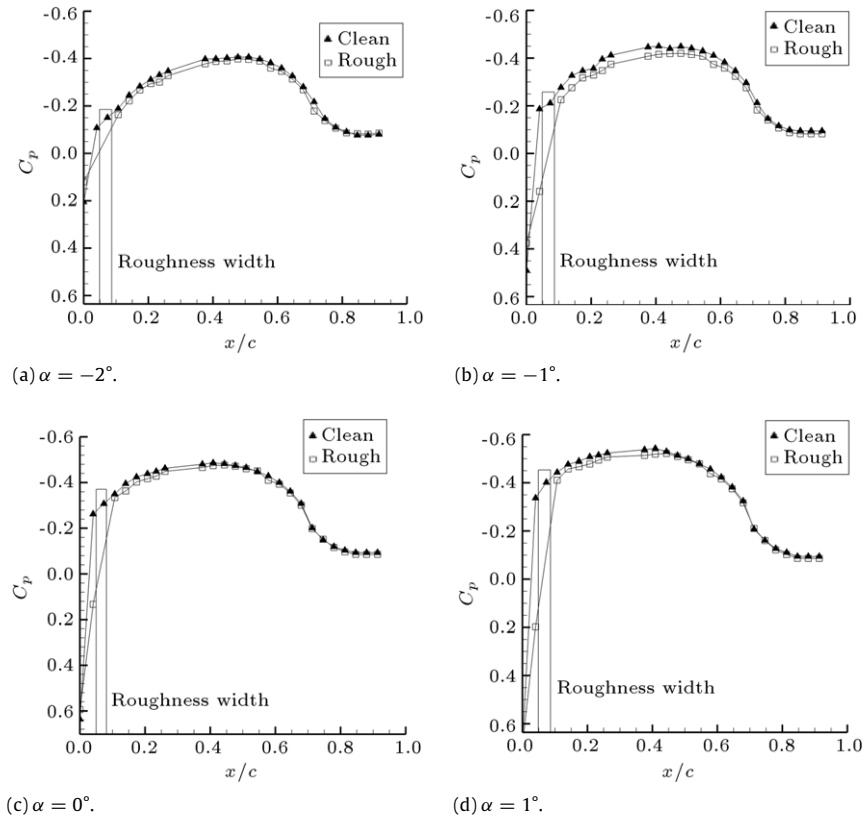


Figure 6: Effect of angle of attack on the middle section pressure distribution,  $v_\infty = 50$  m/s.

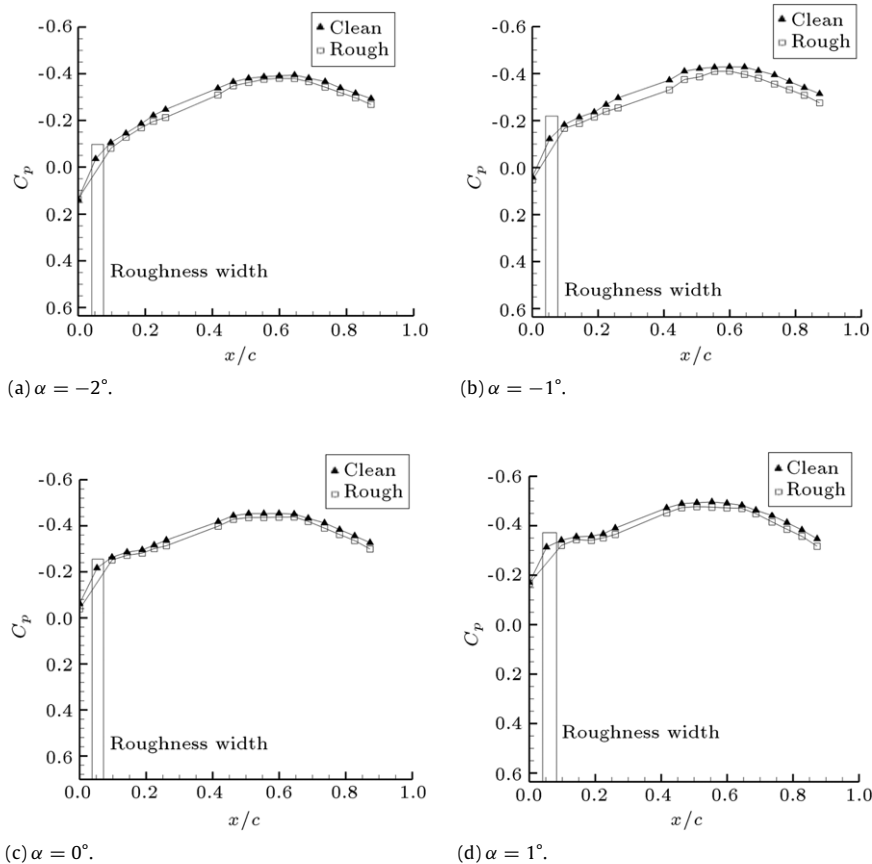


Figure 7: Effect of angle of attack on the outboard section pressure distribution,  $v_\infty = 50$  m/s.

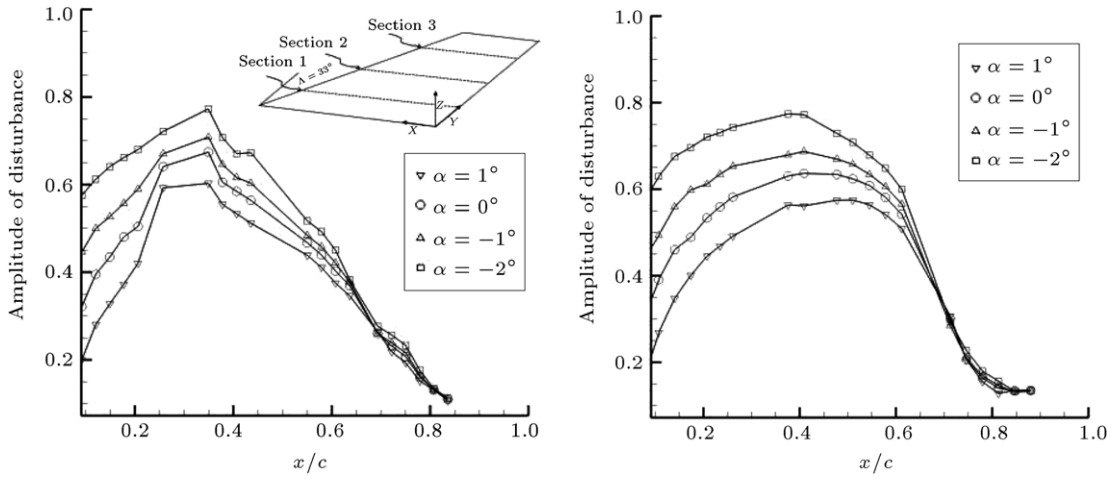
In other words, the disturbances were amplified in a larger interval. Again, for  $x/c > 0.64$ , the disturbances are independent of angles of attack (Figure 8(b)). For the third station, outboard station, close to the wing tip, the amplitude distribution differs significantly from the other two sections. According to Figure 8(c), the point of maximum amplitude of the 3rd station occurs at  $x/c \approx 0.55$ . Therefore, the point of maximum disturbance occurs at a larger  $x/c$  in comparison with the other two sections (Sections 1 and 2), and the disturbances are amplified in a broader region over this section (3rd station). In addition, it seems that the 3rd station amplitude reduction is less than that for the other two sections. However, as seen from Figure 8(c), for the outboard section, the amplitude reduction begins at higher  $x/c$  than that of the other two sections, and since there was no sensor at the end of the airfoil, the zero frequency amplitude distribution could not be measured accurately for the present section (Section 3). It should be noted that it was impossible to install a sensor near the trailing edge since it was very thin.

Therefore, by examining the amplitude distribution shown in Figure 8 for all three sections, it is seen that the zero frequency amplitude distribution has the same trend in all sections (Sections 1 through 3). Zero frequency perturbations begin to amplify near the leading edge and reach their maximum value at some point. By moving further away from the root to the tip of the swept wing, the point of maximum amplitude moves away from the leading edge and the disturbances are amplified on a larger region of the wing upper surface. In addition, the zero frequency amplification regions at the third station are seen to be greater than that of the other two sections (Figure 8(a)–(c)).

Moreover, Figure 8 illustrates that the amplitude of zero frequency increases at all three sections by increasing the angle of attack and confirms that with increasing the angle of attack, the disturbances are amplified. On the other hand, increasing the angle of attack has less influence on the disturbances near the trailing edge, due to the weakening of the zero frequency instability. Especially for the first and second sections (Figure 8(a) and (b)) for  $x/c > 0.6$ , the amplitude of disturbances remains almost constant at all angles of attack examined in this investigation.

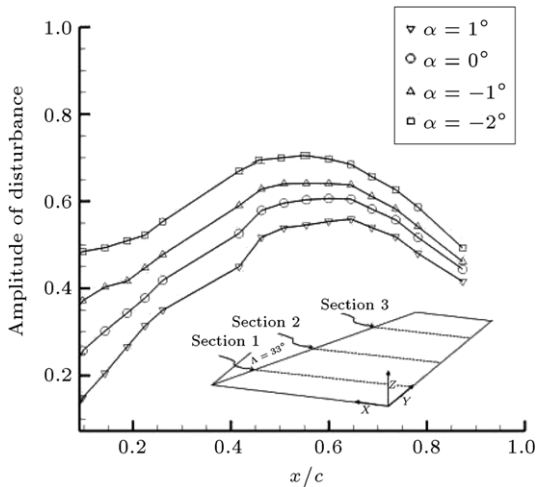
Figure 9 illustrates the zero frequency amplitude distribution at the 1st station, (inboard station), for  $V_\infty = 60$  and 70 m/s. According to this figure, chordwise distributions of the zero frequency amplitude for both freestream velocities of 60, 70 m/s are similar to that of the  $V_\infty = 50$  m/s case, as shown in Figure 8(a). However, in the  $V_\infty = 50$  m/s case (Figure 8(a)), a distortion near  $x/c \approx 0.35$  is seen, which disappears at higher free stream velocities (Figure 9(a) and (b)). At a low freestream velocity, such as the one shown in Figure 8(a) ( $V_\infty = 50$  m/s), a separation bubble could form on the surface of the swept wing. This bubble has affected the sensors located in that vicinity and caused an abrupt fall of the instability distribution along the chord for the 1st station. However, at higher velocities, these effects are negligible, since it seems that the separation bubble has disappeared. Hence, the zero frequency instability distribution has become smoother (Figure 9).

Disturbances in the first stages are formed in the boundary layer with initial amplitude and are then amplified through the boundary layer development over the model. In other



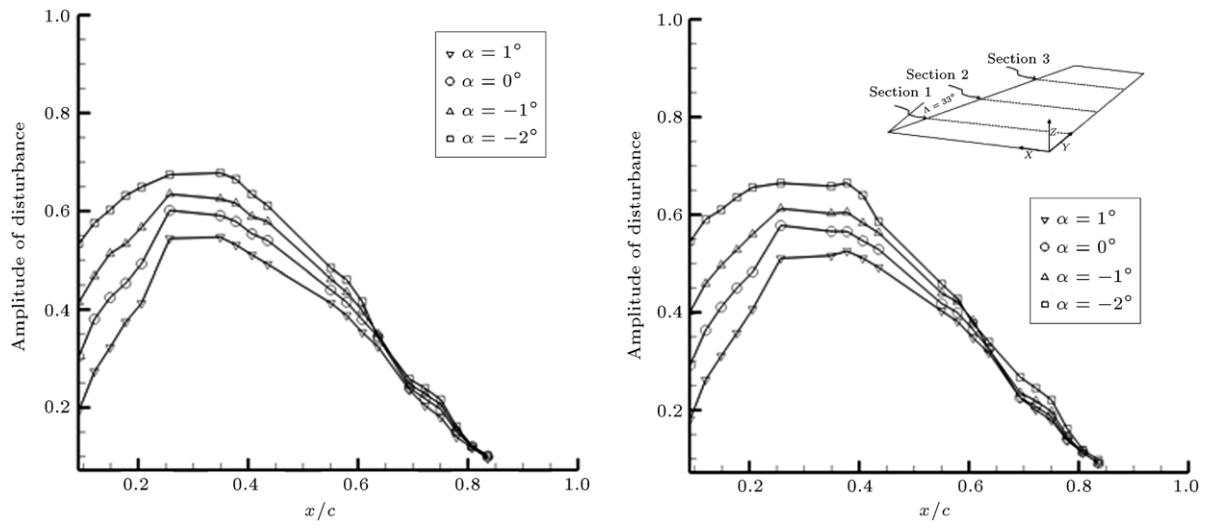
(a) Section 1.

(b) Section 2.



(c) Section 3.

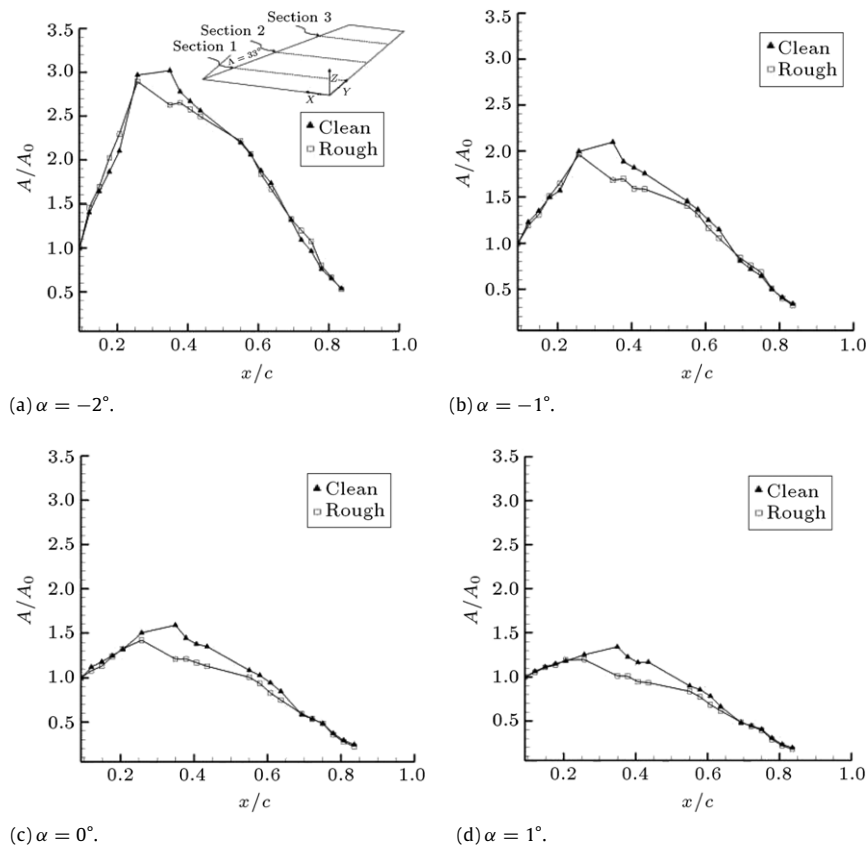
Figure 8: Effect of angle of attack on the amplitude of zero frequency,  $v_\infty = 50$  m/s.



(a)  $V_\infty = 60$  m/s.

(b)  $V_\infty = 70$  m/s.

Figure 9: Effect of angle of attack and free stream velocity on the amplitude of zero frequency at the inboard station.

Figure 10: Zero frequency amplitude ratio at the inboard station,  $v_\infty = 50$  m/s.

words, the instability amplitude variations relative to an initial reference point could specify the instability variation due to the boundary layer development. This means that the zero frequency amplitude ratio ( $A/A_0$ ) distribution along the chord could be used to represent the amplitude of zero frequency at the desired point, relative to the zero frequency amplitude at the 1st measuring point at  $x/c \approx 0.1$ . Since this amplification is due to crossflow stationary instabilities, the ratio could represent the strength of crossflow stationary instabilities over the upper surface of the swept wing.

Figure 10 illustrates chordwise distribution of the zero frequency amplitude ratio at the inboard station for different angles of attack and for a freestream velocity of  $V_\infty = 50$  m/s. According to Figure 10(a), at the 1st section, and for  $\alpha = -2^\circ$ , the disturbances over the rough surface are reduced after an initial amplification, in such a way that around  $x/c \approx 0.5$ , disturbances for the rough surface are even less than those for the clean surface. At other angles of attack, similar results were observed (Figure 10(b) through (d)). In addition, it seems that the instability amplification region over the rough surface at one degree angle of attack (Figure 10(d)), is lower than those for other angles of attack, as shown in Figure 10(a)–(c). In other words, chordwise distribution of the instability over the rough surface at the 1st station is different from that of the clean one. In fact, the zero frequency instability distribution is affected by the favorable pressure gradient area [15] and the roughness has shortened this area at the 1st section. Thus, the effect of roughness on the crossflow stationary instability cannot be studied at the 1st section, due to the narrow instability amplification region. Figure 11 presents roughness influences on the zero frequency instability for the second section for different angles of

attack and for  $V_\infty = 50$  m/s. According to this figure, the amplitude distribution along the chord for both clean and rough surfaces is similar. Thus, the effect of leading-edge roughness on the crossflow stationary instability could be realized better. Figure 11(a) shows that at a few points near the leading edge, and for  $\alpha = -2^\circ$ , there were no significant differences between the rough and clean surface. However, as  $x/c$  is increased, disturbances are gradually amplified. Also, the differences between the two curves continuously increase, in such a way that at the middle region of the 2nd section,  $x/c \approx 0.5$ , the differences are maximized. The disturbances are then weakened at both surfaces and the difference between the two curves is reduced as the trailing edge is approached (Figure 11(a)). However, according to Figure 11(a), roughness elements amplify crossflow zero frequency instabilities at the beginning and middle regions of 2nd section. Similar results for zero frequency instability amplification by leading-edge roughness are also shown in Refs. [9,10].

Figure 11(b) through (d) show the roughness effects on zero frequency instability at the second section for higher angles of attack. From these figures, it is observed that the differences between the two curves reduce as the angle of attack is increased. In fact, roughness effects depend on the boundary layer thickness ( $\delta$ ) [14]. Although the roughness size is constant throughout the tests, the boundary layer thickness increases as the angle of attack is increased. Thus, roughness height to boundary layer thickness ratio ( $k/\delta$ ) was reduced, due to the boundary layer thickness increment. As a result, the roughness influence decreases, as seen from Figure 11.

Figure 12 compares the clean and rough surfaces at the 3rd station for  $V_\infty = 50$  m/s and for different angles of attack. According to Figure 12, the amplitude distribution along the chord

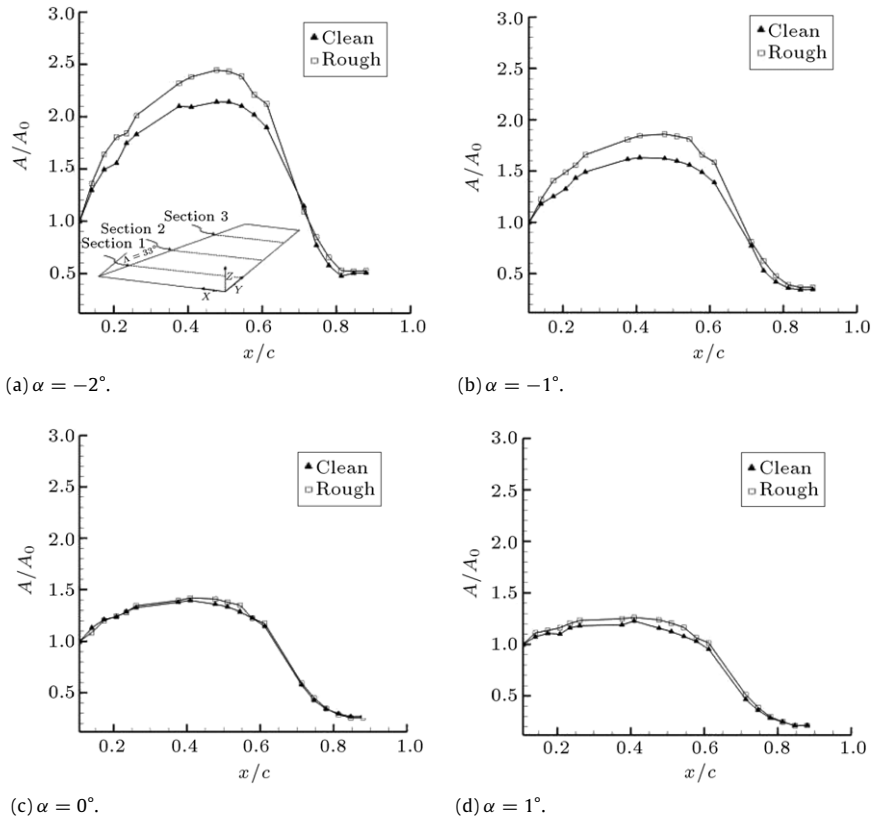


Figure 11: Zero frequency amplitude ratio at the middle section,  $v_\infty = 50$  m/s.

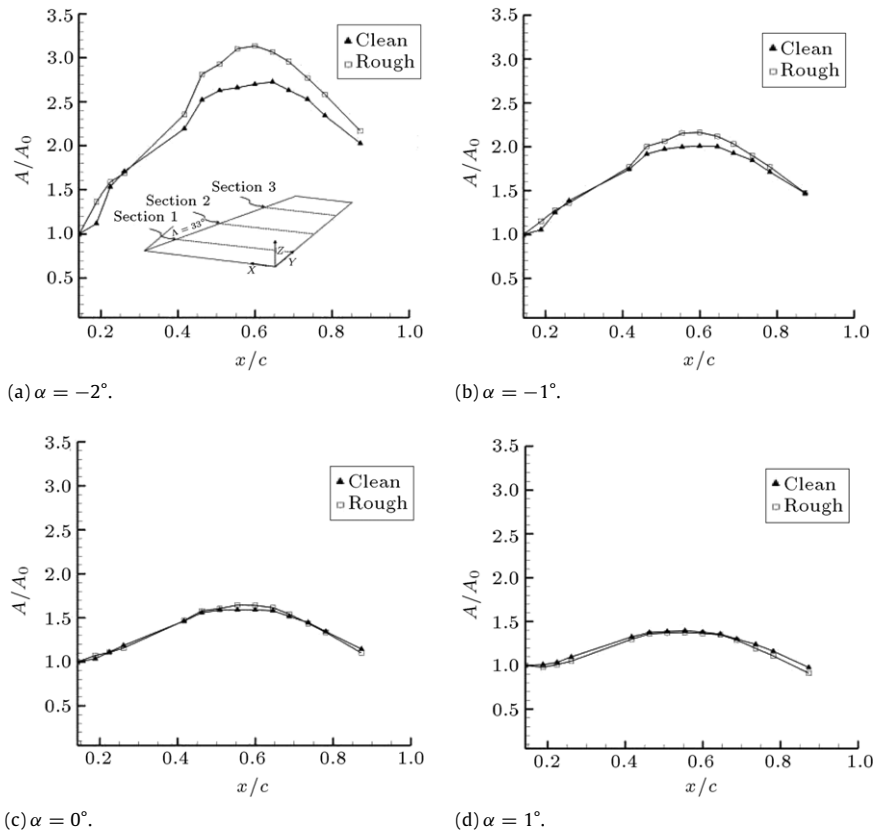


Figure 12: Zero frequency amplitude ratio at the outboard station,  $v_\infty = 50$  m/s.

in both surfaces is very similar at the third station. Thus, similar to the second section, leading-edge roughness effects on the crossflow stationary instability could be investigated. Of course, in the third section, the instabilities are amplified at the larger region in comparison with the second section. At the middle region of the 3rd station and for  $\alpha = -2^\circ$  (Figure 12(a)), roughness amplifies the zero frequency instability. However, since reduction of the disturbances at the third station begins at further distances, there still exist differences between the ends of the outboard station, unlike the other two sections. Figure 12(b) through (d) illustrate the roughness effects on zero frequency instability at the third station for higher angles of attack. According to Figure 12(b) through (d), by increasing angle of attack, the differences diminish, and roughness effects on zero frequency instability decreases. Again, this phenomenon is due to the boundary layer thickness, which is increased, whereas the roughness height is held constant. Thus, roughness influences on zero frequency instability is decreased, as seen from this figure.

#### 4. Conclusion

Wind tunnel tests were performed to examine pressure distribution and zero frequency instability over a semi-span swept wing with a sweep angle of  $33^\circ$ . The investigations were conducted at speeds ranging from 50 to 70 m/s and at angles of attack ranging from  $-2^\circ$  to  $1^\circ$ . Surface pressure data were acquired and compared for both clean and rough surfaces to survey the effect of leading-edge roughness on pressure distribution and on zero frequency instability. The results showed that the roughness elements had little influence on wing surface pressure distribution. In addition, the most influence was observed at the inboard station, where the minimum value of the  $C_p$  was reached. This point occurred at smaller  $x/c$  because of the roughness effects. Further, a spectral analysis of surface pressure signals was used to study stationary crossflow instability and zero frequency over the finite swept wing. The zero frequency amplitude and its variations with roughness elements were investigated at three different chordwise rows. At the inboard station, roughness did not have any effect on the zero frequency instability. At this station (closer to the wing root), the minimum value of the  $C_p$  position was shifted towards the leading edge because of surface roughness. Therefore, zero frequency instability over the rough surface was amplified at a smaller distance along the chord, and roughness did not have a significant influence. However, at the middle and outboard stations, 3-D roughness elements amplified zero frequency instability over the wing upper surface.

Furthermore, zero frequency instabilities at three different stations were compared with each other in order to study the effects of body boundary layer and wing tip flow. The results indicated that at the inboard station, instability was amplified at a smaller region in comparison with the middle one. In addition, comparison of zero frequency instability in the second and third sections indicated that the instability amplification region at the outboard station, closer to the wing tip, was noticeably greater than at the middle station. In other words, by moving further away from the root to the tip of the finite swept wing, the disturbances are amplified over a larger portion of the wing upper surface. In addition, at the third section, the maximum value of the amplitude ratio was increased, with respect to that of the second station.

#### Appendix. Error analysis

Errors in measurements are computed from experimentally measured quantities. Kline and McClintock [16] show that the

uncertainty,  $w_R$ , can be calculated from:

$$R = R(v_1, v_2, \dots, v_n). \quad (\text{A.1})$$

Can be obtained as:

$$w_R = \sqrt{\sum_{i=1}^n \left( \frac{\partial R}{\partial v_i} w_i \right)^2} \quad (\text{A.2})$$

where  $v_i$  are the measured quantities used in the computation of  $R$ , and  $w_i$  is the expected error range for the measured quantities.

In the present experiments, the range of measured quantities is limited to the static and dynamic pressures, measured by the pressure transducers.

The freestream velocity can be obtained from the incompressible Bernoulli equation:

$$U_\infty = \sqrt{\frac{2(p_t - p_\infty)}{\rho_\infty}}, \quad (\text{A.3})$$

where  $p_t$  is total pressure measured by the Pitot tube.

The surface pressure coefficient is obtained:

$$C_p = \frac{p - p_\infty}{q_\infty} = \frac{p_D}{q_\infty}, \quad (\text{A.4})$$

where  $C_p$  is the pressure coefficient and  $p$  is the local surface pressure.

Eq. (A.2) can be applied to Eqs. (A.3) and (A.4) to obtain the uncertainty estimates for  $U_\infty$  and  $C_p$  as:

$$\frac{w_{U_\infty}}{U_\infty} = \sqrt{\left( \frac{w_{p_t}}{2(p_t - p_\infty)} \right)^2}, \quad (\text{A.5})$$

$$\frac{w_{C_p}}{C_p} = \sqrt{\left( \frac{w_{p_D}}{p_D} \right)^2 + \left( \frac{w_{q_\infty}}{q_\infty} \right)^2}. \quad (\text{A.6})$$

Eqs. (A.5) and (A.6) can be applied in a straightforward manner because estimation of the uncertainties involved is easily obtained.

According to the instrument handbook, the uncertainty in the measurement of  $p_t$  in Eq. (A.5) is 0.08% of its reading, but  $q_\infty$  is seen to oscillate due to a very low-frequency modulation of the fan controller at about 1% of its reading.

Thus, the expected maximum uncertainties for  $U_\infty$  and  $C_p$  are calculated to be:

$$\frac{w_{U_\infty}}{U_\infty} = 0.6\%, \quad (\text{A.7})$$

$$\frac{w_{C_p}}{C_p} = 3\%. \quad (\text{A.8})$$

#### References

- [1] Kohama, Y.P. "Three dimensional boundary layer transition study", *Current Science*, 10(6), pp. 800–807 (2000).
- [2] Levchenko, V.Ya. and Scherbakov, V.A. "Instability of a three-dimensional boundary layer on a swept wing", *Journal of Applied Mechanics and Technical Physics*, 38(3), pp. 357–363 (1997).
- [3] Dagenhart, J. "Crossflow stability and transition experiments in a swept-wing flow", PhD thesis, Virginia Polytechnic Institute and state University (1992).
- [4] Deyhle, H. and Bippes, H. "Disturbance growth in an unstable three-dimensional boundary layer and its dependence on initial conditions", *Journal of Fluid Mechanics*, 31(6), pp. 73–113 (1996).

- [5] Bippes, H., Muller, B. and Wagner, M. "Measurements and stability calculations of the disturbance growth in an unstable three-dimensional boundary layer", *Physics of Fluids*, 3(10), pp. 2371–2377 (1991).
- [6] Deyhle, H., Hohler, G. and Bippes, H. "Experimental investigation of instability wave propagation in a Three-dimensional boundary-Layer flow", *AIAA Journal*, 31(4), pp. 637–645 (1993).
- [7] White, E.B., Saric, W.S., Gladden, R.D. and Gabet, P.M. "Stage of swept-wing transition", *39th Aerospace Sciences Meeting & Exhibit*, Reno, NV, AIAA Paper No. 2001-2271 (2001).
- [8] Radeztsky, R.H., Reibert, M.S., Saric, W.S. and Tagaki, S. "Effect of micron-sized roughness on transition in swept-wing flows", *31th Aerospace Sciences Meeting & Exhibit*, Reno, NV, AIAA Paper No. 93-0076 (1993).
- [9] Radeztsky, R.H., Reibert, M.S. and Saric, W.S. "Development of stationary crossflow vortices on a swept wing", AIAA Paper No. 94-2373 (1994).
- [10] Reibert, M.S., Saric, W.S., Carrillo Jr., R.B. and Chapman, K.L. "Experiments in nonlinear saturation of stationary crossflow vortices in a swept-wing boundary layer", AIAA Paper No. 96-0184 (1996).
- [11] Carrillo Jr., R.B. "Distributed-roughness effects on stability and transition in swept-wing boundary layers", Master's Thesis, Arizona State University (1996).
- [12] White, E.B. and Saric, W.S. "Application of variable leading-edge roughness for transition control on swept wings", AIAA Paper No. 2000-0283 (2000).
- [13] Beckwith, T.G., Marangoni, R.D. and Lienhard, J.H., *Mechanical Measurements*, 5th Edn., Addison-Wesley Publishing Company (1993).
- [14] White, F.M., *Viscous Fluid Flow*, 3rd Edn., Mc Graw-Hill, New York (2006).
- [15] Lin, R.S. "Stationary crossflow instability on an infinite swept wing", PhD thesis, Arizona State University (1992).
- [16] Rathakrishnan, E., *Instrumentation Measurement and Experiments in Fluids*, 1st Edn., Taylor and Francis group (2007).

**Mohammad Reza Soltani** has a Ph.D. degree in Aerodynamics from the University of Illinois at Urbana-Champaign, USA, and is currently Professor in the Aerospace Engineering Department of Sharif University of Technology, Tehran, Iran. His research interests include: applied aerodynamics, unsteady aerodynamics wind tunnel testing, wind tunnel design, and data processing.

**Mehran Masdari** received his B.S. degree in Aerospace Engineering and M.S. and Ph.D. degrees in Aerodynamics from Sharif University of Technology, Tehran, Iran, in 2000, 2003 and 2010, respectively. He is currently assistant lecturer at Tehran University, Iran. His research interests include: applied aerodynamics, wind tunnel testing, neural network and data processing.

**Hamid Damghani** received his B.S. degree in Mechanical Engineering from Bahonar University, Iran, in 2007, and an M.S. degree in Propulsion from Sharif University of Technology, Tehran, Iran, in 2010. His research interests include: experimental aerodynamics and optical measurements.